Mean Climate and Variability of the Atmosphere and Ocean on an Aquaplanet

JOHN MARSHALL, DAVID FERREIRA, J.-M. CAMPIN, AND DANIEL ENDERTON

Department of Earth, Atmospheric, and Planetary Sciences, Massachusetts Institute of Technology, Cambridge, Massachusetts

ABSTRACT

Numerical experiments are described that pertain to the climate of a coupled atmosphere–ocean–ice system in the absence of land, driven by modern-day orbital and CO_2 forcing. Millennial time-scale simulations yield a mean state in which ice caps reach down to 55° of latitude and both the atmosphere and ocean comprise eastward- and westward-flowing zonal jets, whose structure is set by their respective baroclinic instabilities. Despite the zonality of the ocean, it is remarkably efficient at transporting heat meridionally through the agency of Ekman transport and eddy-driven subduction. Indeed the partition of heat transport between the atmosphere and ocean is much the same as the present climate, with the ocean dominating in the Tropics and the atmosphere in the mid–high latitudes. Variability of the system is dominated by the coupling of annular modes in the atmosphere and ocean. Stochastic variability inherent to the atmospheric jets drives variability in the ocean. Zonal flows in the ocean exhibit decadal variability, which, remarkably, feeds back to the atmosphere, coloring the spectrum of annular variability. A simple stochastic model can capture the essence of the process. Finally, it is briefly reviewed how the aquaplanet can provide information about the processes that set the partition of heat transport and the climate of Earth.

1. Introduction

In an attempt to improve our understanding of the nature of the interaction between the atmosphere and ocean in setting the climate of the planet, we have begun a series of highly idealized geophysical fluid dynamics (GFD) experiments with a numerical model of the coupled atmosphere–ocean–ice system. Our goal is not to simulate the present climate, or that of any other period in Earth history. Rather, it is to study the details of a coupled system in which complications of geography/land–sea distribution are simplified—and in the present aquaplanet entirely removed—but in which the requisite fluid dynamics are well described. In this way the coupling of the two fluids can be studied in its most elemental form. Here we explore the extreme limit of a planet, which in all other respects is like the present Earth, except there is no land. It is entirely covered with an ocean of uniform depth of 5.2 km. Above the ocean there is an atmosphere that is energized by in-

coming solar radiation. Furthermore, if conditions permit, ice can form.

Before going on, it should be mentioned that to atmospheric modelers, more often than not, "aquaplanet" is taken to imply an atmosphere coupled to a slab ocean or even a prescribed sea surface temperature (SST) distribution, in the absence of land. For example, Hess (1993) uses an aquaplanet configuration with prescribed SSTs to investigate the sensitivity of the intertropical convergence zone (ITCZ) to various latitudinal distributions of SST; Kirtman and Schneider (2000) and Barsugli et al. (2005) couple an atmosphere to a thermodynamic ocean model and show that tropical precipitation is sensitive to the mean state in the Tropics. Here we use aquaplanet to mean the full coupling of an atmospheric model to an ocean model, both of which represent dynamics and so can transport properties around the globe. Such calculations have rarely been carried out before. In particular, we are only aware of one published study[1] of a coupled aquaplanet configu-

Corresponding author address: Dr. John Marshall, Dept. of Earth, Atmospheric, and Planetary Sciences, Massachusetts Institute of Technology, Green Building, Rm. 1526, Cambridge, MA 02139-4307.
E-mail: jmarsh@mit.edu

[1] An interesting historical note, brought to our attention by E. Schneider, is the unpublished study by J. Charney and collaborators at MIT during the late 1970s: see Charney et al. (1988), a NASA technical memorandum published after Charney's death. This describes a coupled system on an aquaplanet with represen-

ration, that of Smith et al. (2006). There the emphasis was on the role of ocean circulation in the coupled system, and in particular the importance of geometrical constraints (such as the absence or presence of meridional boundaries) on the ability of the ocean to transport heat around the globe. The pure aquaplanet considered in this paper (i.e., in the complete absence of any topographic constraints) is the same as the reference configuration reported in Smith et al. (2006), but with rather significant differences in ocean model formulation which lead, it turns out, to very different climate states. Our respective equilibrium solutions are compared as appropriate.

In section 2 we describe the mean state of the coupled system obtained by integrating forward our numerical model. From what we know of climate dynamics, one might expect—and indeed one finds—that the atmosphere of the aquaplanet is not dissimilar to our own. Differential heating/cooling sets up atmospheric wind systems: we observe a tropical Hadley regime and midlatitude jet streams that break down due to baroclinic instability. Cooling over the poles leads to the formation of ice caps, which extend down to a latitude of 55° in both hemispheres (see Fig. 1). Momentum transport by atmospheric synoptic systems support westerly winds in mid–high latitudes and easterlies in tropical latitudes. These winds blow over the ocean, bringing it into motion.

The absence of boundaries in the ocean, however, yields an ocean circulation pattern that is very different from our own. It comprises zonal jets whose direction is set by that of the prevailing winds above. We observe easterlies in the tropical belt and westerlies in mid–high latitudes. The dynamics of these zonal jets is reminiscent of that of the present-day Antarctic Circumpolar Current. The structure of the thermocline is controlled by eddy processes that (due to the tiny Rossby deformation radius in the ocean) must be parameterized rather than resolved. The meridional overturning circulation (MOC) of the ocean is entirely associated with the wind and eddy-driven subduction—there is no "thermohaline circulation" driven convectively from the pole. The MOC comprises residual-mean oceanic "subtropical" cells (STCs) that extend from the equator up to the midlatitudes. Together the atmosphere and ocean carry heat from the equator to the pole. We find that the partition of heat transport between the atmosphere and ocean is remarkably similar to the present climate. We discuss why this is so.

tation of atmosphere and ocean dynamics, but in an axisymmetric configuration designed to study factors that control the position of the ITCZ over the ocean.
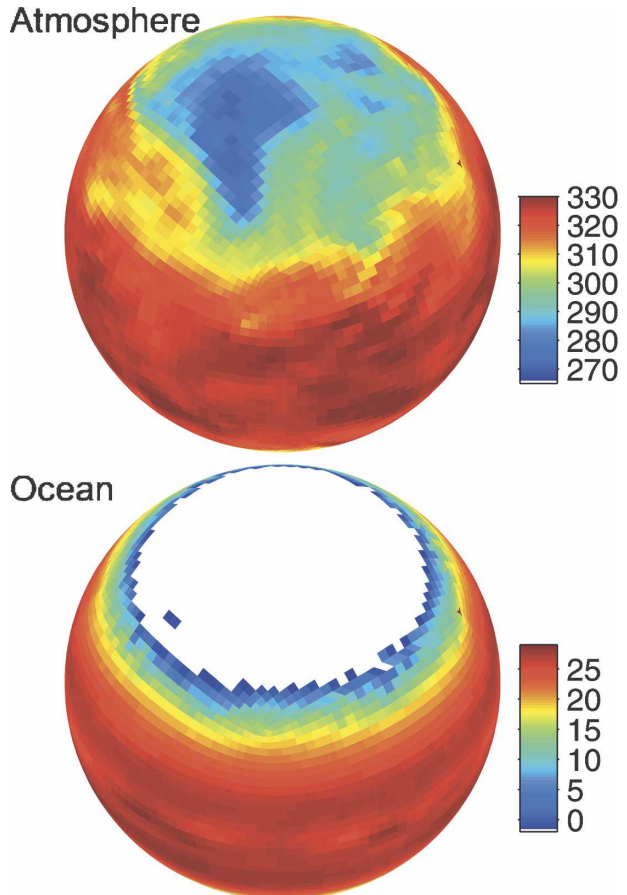

FIG. 1. (top) A snapshot of atmospheric temperature (K) at 500 mb revealing the presence of synoptic systems. (bottom) The SST (°C) and ice distribution. The underlying cubed sphere grid can be seen.

In section 3 we describe the variability observed in the coupled system. Because of the absence of meridional boundaries, there are no persistent east–west temperature gradients and the "ENSO" phenomenon is absent. The leading modes of variability are midlatitude "annular modes" in which the atmospheric westerlies fluctuate in both strength and position (Thompson and Wallace 1998). This leads to changes in the zonal wind stress that also set up annular modes in the zonal jets of the ocean. The ultimate source of the variability of the coupled system is the "shake" due to the interaction between atmospheric synoptic systems with the atmospheric zonal jet. However, we find that coupling between the annular modes in the two fluids leads to a distinct decadal signal in both fluids. A simple stochastic model of the observed variability is developed and captures the essence of the coupled mechanism. In section 4 we conclude, emphasizing what we have learned, which transcends the model used.

2. The coupled model

The coupled model used in this study is the Massachusetts Institute of Technology general circulation model (MITgcm; Marshall et al. 1997a,b). Fluid isomorphisms are employed to render atmospheric and oceanic models from one hydrodynamical core, as discussed in Marshall et al. (2004). As described in Adcroft et al. (2004), the atmosphere and ocean are integrated forward on the same "cubed sphere" horizontal grid at C32 (each face of the cube is split in to a 32 × 32 matrix of cells) yielding a resolution of, nominally, 2.8° of latitude. The use of the cubed sphere avoids problems associated with the converging meridians of a latitude–longitude grid and ensures that the model dynamics at the poles are treated with as much fidelity as elsewhere.

The atmosphere is of "intermediate" complexity and comprises five vertical levels and employs the Simplified Parameterization, Primitive Equation Dynamics (SPEEDY) physics package described in Molteni (2003), comprising a four-band radiation scheme, a parameterization of moist convection, a boundary layer scheme, and resolved baroclinic eddies. More details can be found in appendix A. The ocean model has 15 vertical levels spread over the flat-bottomed, 5.2-km-deep ocean, increasing from 50 m in the surface layers to 690 m in the abyss. Diapycnal mixing is represented with a constant diffusivity of 3×10^{-5} m^2 s^{-1}, somewhat larger, but broadly in accord with observed values of mixing in the ocean thermocline. Due to our choice of a flat-bottom ocean, topographic form drag plays no role in balancing momentum input from the wind, whereas mountain drag is the primary momentum sink in the Antarctic Circumpolar Current of the present climate. To avoid the generation of strong barotropic zonal flows, therefore, we employ an enhanced bottom friction (linear drag) parameter that is tuned to damp abyssal currents toward zero. The model parameterizes eddies as an advective and stirring process, using the scheme of Gent and McWilliams (1990) with a transfer coefficient of 800 m^2 s^{-1}. Convective adjustment, implemented as an enhanced vertical mixing of temperature (T) and salt (S), is used to represent ocean convection. A thermodynamic ice model following Winton (2000) is also incorporated into the model. Orbital forcing and CO_2 levels are prescribed at present-day values. The seasonal cycle is represented: there is no diurnal cycle.

The whole system is integrated forward on a parallel computer, one processor being employed for each side of the atmospheric cube: one for the ocean and one to handle coupling. The system can carry out 1000 yr of synchronous coupled integration in two weeks of dedicated integration. Fluxes of momentum, heat, and freshwater are exchanged every hour (the ocean model time step). The model, launched from a state of rest with temperature and salinity distributions taken from a zonal-average ocean climatology, has been integrated out for 4000 yr to a quasi-equilibrium [abyssal temperatures are drifting by $\sim 0.1°C$ (100 yr)$^{-1}$], which has no knowledge of the initial conditions. We now describe the mean state of the coupled model obtained by averaging fields over the final 100 yr of the integration.

a. Mean state

1) DISTRIBUTION OF TEMPERATURE, MOISTURE, SALT, WINDS, AND CURRENTS

Figure 2a (top left) shows the zonal average potential temperature in the atmosphere. We see a tropical region of weak horizontal temperature gradient with, on its poleward flanks, a broad baroclinic zone extending up to the poles in each hemisphere. The poles are very cold (reaching 250 K) and indeed are covered in ice down to latitudes of $\sim 55°$. This is very evident in Fig. 2a (bottom left), which shows the zonal average temperature in the ocean. In polar regions below the ice we see a temperature inversion in the top few 100 m, which is salinity compensated (see Fig. 2b, bottom left). The main thermocline of the aquaplanet ocean is not that dissimilar from our own. We observe a warm lens of fluid bulging down into the subtropics to a depth of ~ 1 km and markedly thinning in equatorial latitudes coinciding with bands of upwelling. The ocean is well mixed beneath the thermocline and the poles with abyssal temperatures of $\sim 2°C$. Upwelling at high latitudes draws well-mixed abyssal fluid up toward the surface.

Figure 2a shows the zonal average zonal winds (top right) and currents (bottom right). Away from boundary layers and the equator, they are in thermal wind balance with the meridional temperature gradients seen in Fig. 2a (left). We observe subtropical westerly jet streams reaching 30 m s^{-1} at 250 hPa and easterlies in equatorial latitudes. At the surface (see Fig. 3, top) we see surface westerlies exerting an eastward zonal stress on the ocean poleward of 30°, with trade winds exerting a westward stress on either side of the equator. It is worthy of note that there are no polar easterlies. Because of the absence of coasts, the ocean comprises zonal jets that flow in the same sense as the stress applied at the surface. They are in thermal wind balance with tilted buoyancy surfaces in the interior of the ocean. As discussed in section 2b, the wind stress is carried down the water column by (parameterized) eddy form drag where it is ultimately balanced by ocean
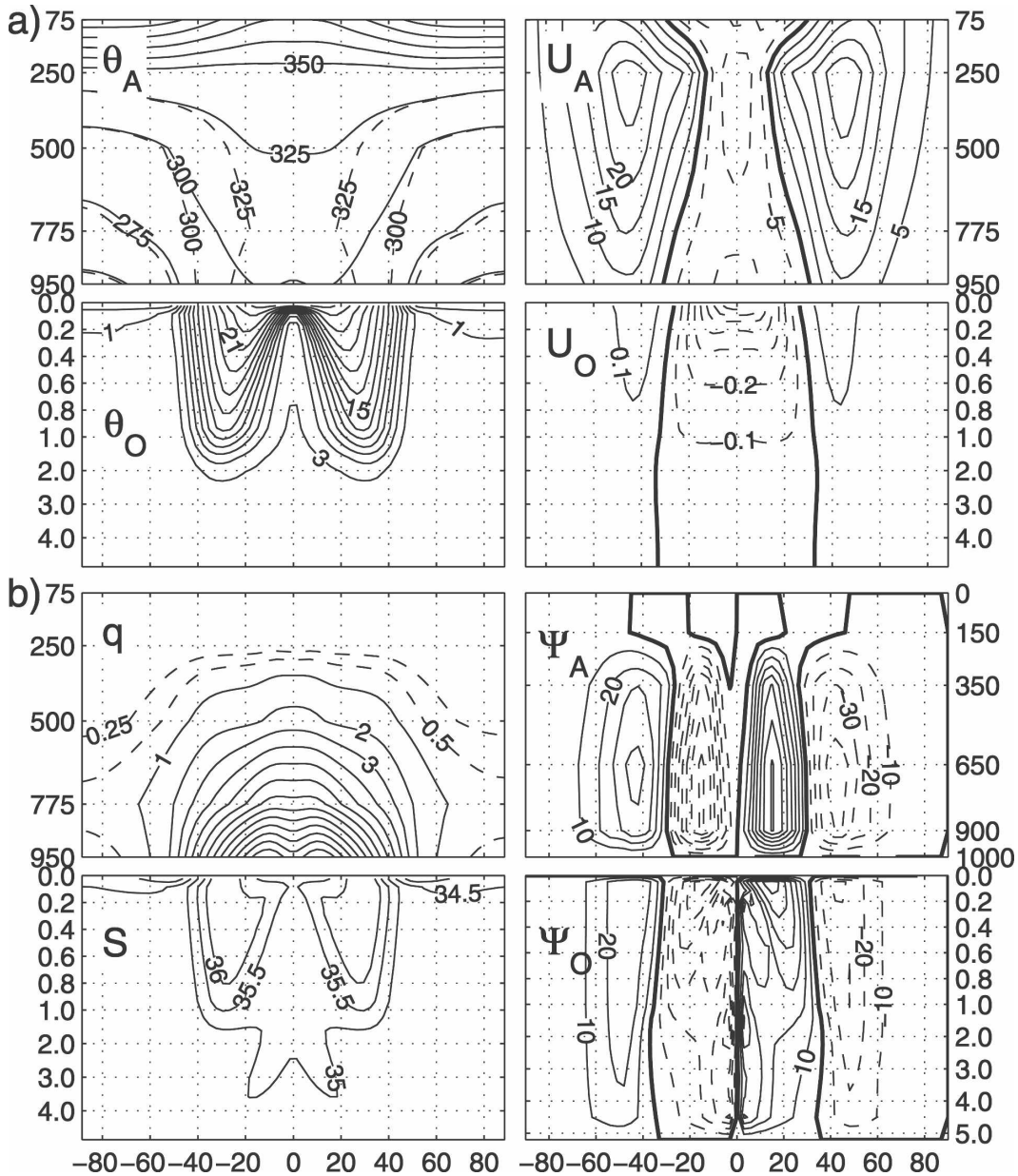
FIG. 2. Time-mean, zonally averaged (a) (left) potential temperature (solid line) and moist potential temperature (dotted line) in the atmosphere (top, K) and ocean (bottom, °C) and (right) zonal wind in the atmosphere (top, m s^{-1}) and ocean (bottom, in m s^{-1}). (b) (left) Specific humidity q (top, g kg^{-1}) and salinity S (bottom, in psu) and (right) Eulerian-mean overturning circulation in the atmosphere (top, Sv $\equiv 10^9$ kg s^{-1}) and for the ocean (bottom, Sv). A positive streamfunction denotes a clockwise circulation.

bottom stress. Westward-flowing surface currents along the equator reach 0.8 m s^{-1}; eastward-flowing currents in the midlatitudes reach speeds of 0.2 m s^{-1}.

The geometry of the buoyancy surfaces in the ocean is controlled by the pattern of surface stress. The Ekman pumping field set by the curl of this stress pattern explains the large-scale undulations in the subsurface thermocline seen in Fig. 2a (bottom left), with up-

welling of cold water in a tropical band demarcated by the zero curl line at ±20°. Downwelling between latitudes 20° and 45° pumps warm water down from the surface.

The moisture and salinity fields of the coupled system are shown in Fig. 2b. The specific humidity (top left) is large where the air is warm, reaching 15 g kg^{-1} at low levels in the Tropics. It decays with height and
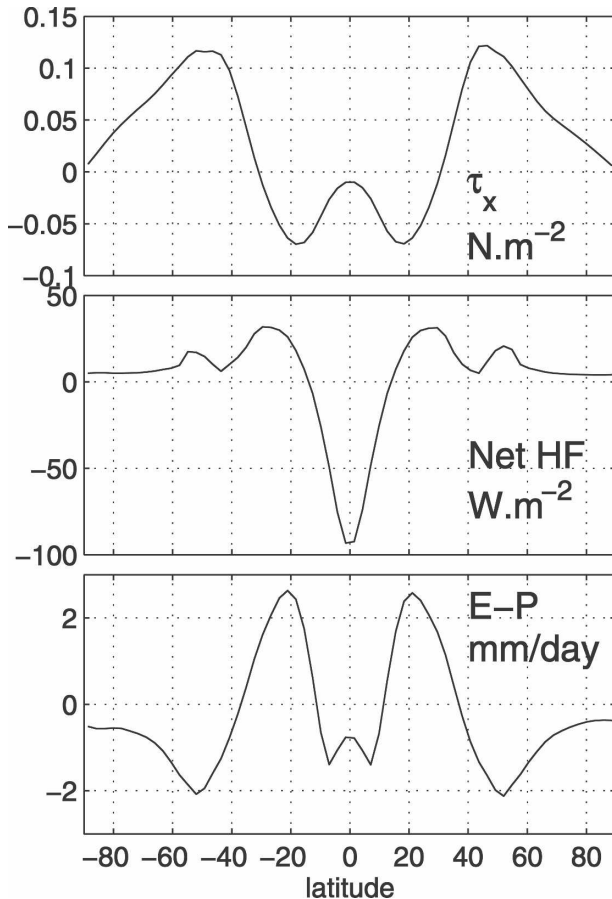
FIG. 3. The zonal-average (top) zonal surface stress in N m^{-2}, (middle) net heat flux in W m^{-2} (negative is into the ocean), and (bottom) freshwater flux $(E - P)$ in mm day^{-1}.

latitude. Its "mirror image," the salinity field (bottom left) in the ocean, exhibits saline tongues where (see Fig. 3, bottom) evaporation exceeds precipitation in the subtropics. The excess of precipitation over evaporation in the Tropics and high latitudes leads to a salinity minimum at these latitudes. In particular, we observe very fresh water beneath the ice that stabilizes the temperature inversion observed there.

2) MERIDIONAL OVERTURNING CIRCULATION

The Eulerian meridional overturning circulation, $\overline{\psi}_{A,O}$, in the two fluids is shown in Fig. 2b (right). In the atmosphere we observe Eulerian-mean Hadley cells symmetrically arranged around the equator, with Ferrel cells in mid- and high latitudes. It is interesting to observe that the Eulerian-mean overturning circulation in the ocean, $\overline{\psi}_O$, has exactly the same pattern and sense as in the atmosphere. To the extent that lateral eddy momentum fluxes due to large-scale eddies (parameterized in the ocean, resolved in the atmosphere) can be

neglected in the boundary layers of the two fluids, then one would expect that $\overline{\psi}_A = \overline{\psi}_O$. This is indeed observed in the Tropics (the Hadley regime) but not to the same degree in midlatitudes where $\overline{\psi}_A$ exceeds $\overline{\psi}_O$ by about 50% because eddy momentum fluxes associated with synoptic eddies cannot be neglected.[2] Even here, though, the Eulerian overturning strengths in the two fluids are of the same order. We will see in section 2c, however, that the eddy-driven mass (bolus) transport in the atmosphere is very much stronger than typical overturning strengths in the ocean, a fact that has great importance for the partition of heat transport between the two fluids.

Figure 4 shows the components of the overturning circulation in the ocean in more detail. The eddy-induced circulation, ψ_O^*, tends to oppose the Eulerian mean, $\overline{\psi}_O$, so that the residual flow,

$$\psi_{O_{\text{res}}} = \overline{\psi}_O + \psi_O^*, \qquad (1)$$

as its name suggests, is smaller in an absolute sense than the terms that make it up (see Fig. 4, bottom). This may be interpreted as follows. The pattern of surface wind stress pumps the surface buoyancy distribution down in to the subtropics and sucks up abyssal values toward the surface in the Tropics and high latitudes. This tilts $\overline{b}$ surfaces creating a store of available potential energy for baroclinic instability that acts to flatten out the mean buoyancy surfaces, $\overline{b}$, counteracting the wind, as first described in Gill et al. (1974). Thus, ψ_O^* acts in the opposite sense to $\overline{\psi}_O$, partially cancelling it out. This cancellation is rather complete in mid–high latitudes (see Fig. 4, bottom).

It is also of note that there is no deep meridional overturning circulation in the ocean emanating from polar latitudes. Although the polar oceans are weakly stratified, a deep-reaching thermohaline circulation driven by polar sinking is not present.

b. Dynamical interpretation

A simple model of oceanic zonal flows such as the Antarctic Circumpolar Current, has been developed by Marshall and Radko (2003) that, in appropriately modified form, can be used to rationalize the mean oceanic state of the aquaplanet ocean.

The zonal-average, residual-mean momentum equation can be written thus

$$-f v_{O_{\text{res}}} = \frac{1}{\rho_O} \left[\left(\frac{\partial \tau}{\partial z} + \frac{\partial \tau_e}{\partial z} \right) + A_h \nabla^2 u_{O_{\text{res}}} \right], \qquad (2)$$

----

[2] In all plots of meridional overturning streamfunction we use a Sverdrup (Sv) redefined as a mass transport equivalent to $\rho_O \times 1$ Sv of volume transport $= 10^3$ kg m$^{-3} \times 10^6$ m^3 s$^{-1} = 10^9$ kg s^{-1}.
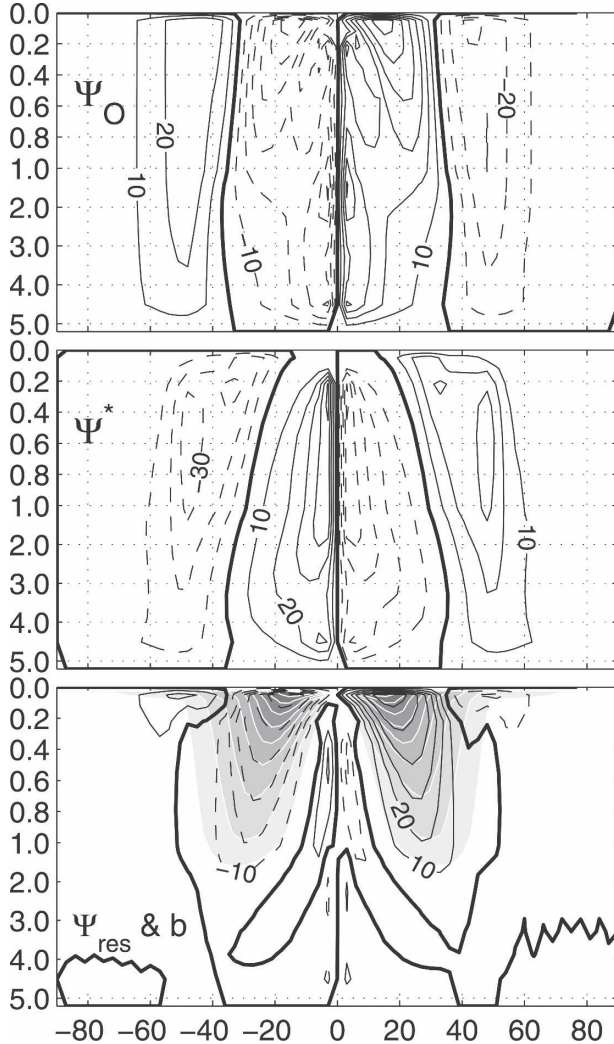
FIG. 4. Components of the time-mean, zonally averaged over-turning circulation in the ocean $\psi_{O_{res}} = \overline{\psi}_O + \psi_O^*$ (Sv): (top) Eulerian-mean $\overline{\psi}_O$, (middle) bolus transport ψ_O^*, and (bottom) residual transport $\psi_{O_{res}}$. The buoyancy field, represented by the grayscale and the white lines, is superimposed.

where τ are the applied stresses (surface and bottom), and

$$\tau_e = \rho_O f \frac{\overline{v'b'}}{\partial \overline{b}/\partial z} = \rho_O f K s_\rho = \rho_O f \psi_O^*, \qquad (3)$$

is the parameterized eddy stress, expressed in terms of the bolus streamfunction $\psi_O^* = K s_\rho$, where K is an eddy transfer coefficient ($\overline{v'b'} = -K \partial \overline{b}/\partial y$), and $s_\rho = -(\partial \overline{b}/\partial y)/(d\overline{b}/dz)$ is the slope of mean buoyancy surfaces. This is the residual-mean interpretation of the Gent and McWilliams (1990) parameterization (see Ferreira et al. 2005). Note that in Eq. (2) we also include a term $A_h \nabla^2 u_{O_{res}}$, representing horizontal mixing

of momentum that is required in the model to describe frictional (Munk 1950) boundary layers associated with western boundary currents.[3]

Integrating Eq. (2) w.r.t. height and noting that at the sea surface $\tau = \tau_s$, the surface wind stress, $\tau_e = 0$ and $\psi_{O_{res}}(0) = 0$, we obtain

$$\psi_{O_{res}}(y, z) = \underbrace{-\frac{1}{\rho_O} \frac{\tilde{\tau}}{f}}_{\overline{\Psi}_O} + \underbrace{K s_\rho}_{\Psi_O^*}, \qquad (4)$$

where

$$\tilde{\tau} = \tau_s + \int_{-z}^{0} A_H \nabla^2 u_{O_{res}} \, dz \qquad (5)$$

is the mean stress divergence resulting from the wind and small-scale lateral mixing processes over the depth range $-z \rightarrow 0$.

If lateral momentum mixing were negligible, then $\tilde{\tau} = \tau_s$ and so $\overline{\Psi}_O$ would be independent of depth, and the transport of the surface and bottom Ekman layers would be equal and opposite. However, from Fig. 4 (top) one can see that the $\overline{\Psi}_O$ contours vary rather markedly with depth in the interior, attesting to the nonnegligible role of viscosity in the momentum balance of the model.

The zonal average of the residual-mean buoyancy equation is

$$J(\psi_{O_{res}}, \overline{b}) = \frac{\partial \mathcal{B}}{\partial z}, \qquad (6)$$

where $\mathcal{B}$ are (parameterized) fluxes of buoyancy due to small-scale processes and air–sea fluxes. In the interior one might expect $\partial \mathcal{B}/\partial z$ to be small resulting in a coincidence of $\psi_{O_{res}}$ and $\overline{b}$ contours. This is tested in Fig. 4 (bottom) where we have superimposed $\overline{b}$ (the grayscale and white contours) on $\psi_{O_{res}}$. We do indeed observe a functional relationship that must be set by surface processes. Arguments presented in Marshall (1997) suggest that $\psi_{O_{res}} = -\mathcal{B}_s/\overline{b}_y$, where $\mathcal{B}_s$ is the net air–sea buoyancy flux and $\overline{b}_y$ is the meridional buoyancy gradient at the sea surface. However, in our numerical model, due to the presence of near-surface mixing processes, such a simple relationship is not found to be useful. Instead we now make direct use of the $\psi_{O_{res}}(\overline{b})$ observed in the model to solve for the structure of the thermocline.

---

[3] Note that in the present simulation, in which there are no meridional boundaries, western boundary currents do not exist. However, in subsequent studies (described elsewhere) we introduce a north–south boundary permitting Sverdrup dynamics and ocean gyres and so demanding lateral momentum mixing terms.
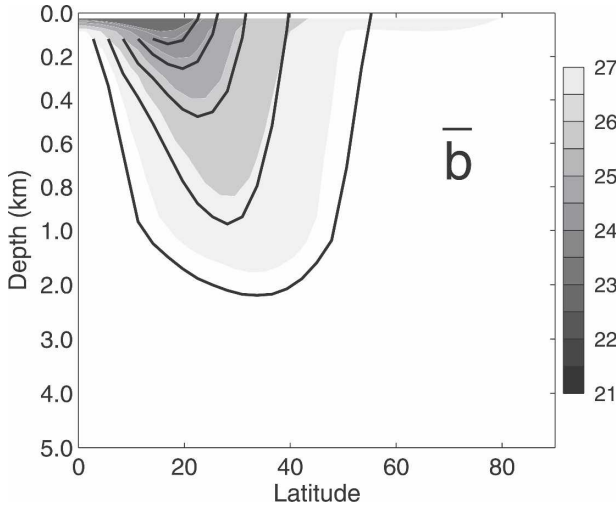
FIG. 5. Solutions for $\bar{b}$ (black lines) obtained by integrating Eq. (7) down from the surface using the method of characteristics described in Marshall and Radko (2003). These are to be compared to the buoyancy field from the ocean model (shown by the white lines and gray shading; units are in kg m^{-3}).

Rearranging Eq. (4) to make the slope of buoyancy surfaces the subject of the equation, we find

$$s_\rho = \frac{1}{K}\left[\psi_{O_{res}}(\bar{b}) + \frac{1}{\rho_O}\frac{\tilde{\tau}}{f}\right]. \qquad (7)$$

Given the $\bar{b}$ distribution at the surface and the observed functional relationship, $\psi_{O_{res}}(\bar{b})$, solutions for $\bar{b}$ can be obtained by integrating Eq. (7) down from the surface using the method of characteristics described in Marshall and Radko (2003). In Fig. 5, the solution thus obtained is compared with the buoyancy field of the model. There is encouraging agreement showing that the simple dynamical balance given in Eq. (7), which is at the heart of Marshall and Radko's (2003) theory of the ACC and its overturning circulation, is appropriate to the aquaplanet ocean. It should be emphasized that Eq. (7) is radically different from classical Sverdrup balance that is clearly not applicable to our aquaplanet in the absence of meridional barriers. Here, the depth of the thermocline is fundamentally controlled by eddy processes, as described in Marshall et al. (2002).

c. Heat transport in the coupled system

The meridional heat transport in the coupled model is presented in Fig. 6. We see that the model atmosphere and ocean together transport 8 PW poleward, peaking at ±40° of latitude. As noted in Czaja and Marshall (2006), the partition of heat transport between the atmosphere and ocean in the aquaplanet simulation is remarkably similar to that of the present
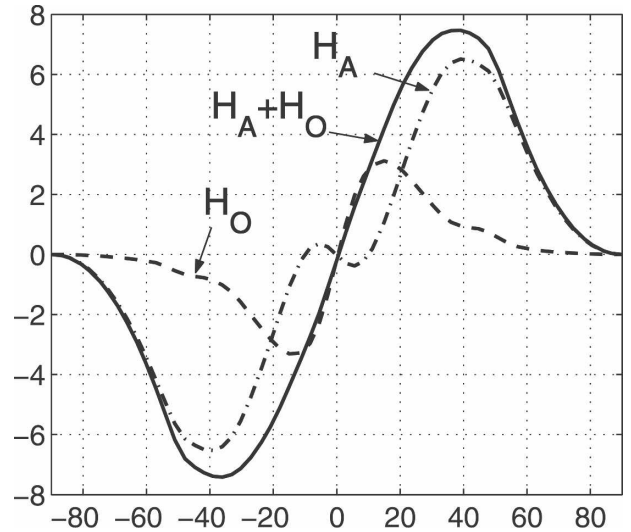

FIG. 6. The total meridional energy transport (PW) on the aquaplanet and the contributions from the atmosphere and ocean.

climate, with the atmosphere dominating in mid–high latitudes and the ocean dominating in the Tropics.

Useful insights in to the mechanisms of heat transport in the two fluids can be obtained by writing the meridional heat transport thus (in this case for the ocean):

$$\rho_o c_o \int_{-H}^{0} v_{O_{res}}\vartheta \, dz = -c_o\rho_O \int_{-H}^{0} \frac{\partial\psi_{O_{res}}}{\partial z}\vartheta \, dz$$

$$= c_o\rho_O \int_{-H}^{0} \psi_{O_{res}}\frac{\partial\vartheta}{\partial z}\, dz$$

$$= \int_{B_{bottom}}^{B_{top}} \Psi_{O_{res}}\, dB, \qquad (8)$$

where ϑ is the potential temperature and we have noted that $\psi_{O_{res}} = 0$ at the limits of integration, made use of the mass transport streamfunction $\Psi_{O_{res}} = \rho_O\psi_{O_{res}}$ (units of kg s^{-1}) and employed a scaled potential temperature (which we can liken to a Bernoulli function) $dB = c_o d\vartheta$ (units of J kg^{-1}): see also Schneider et al. (2006) for a discussion of isentropic diagnostics of the general circulation. It is clear from Fig. 7, where we plot the contributing terms in the ocean heat transport, that Eulerian and bolus contributions oppose one another, with diffusive processes [neglected in Eq. (8)] making only a small contribution. An analogous expression to Eq. (8) can be written down for the atmosphere (see Czaja and Marshall 2006) where now dB is interpreted as a change in moist static energy.

Equation (8) suggests that a key to rationalizing the processes that contribute to meridional energy trans-
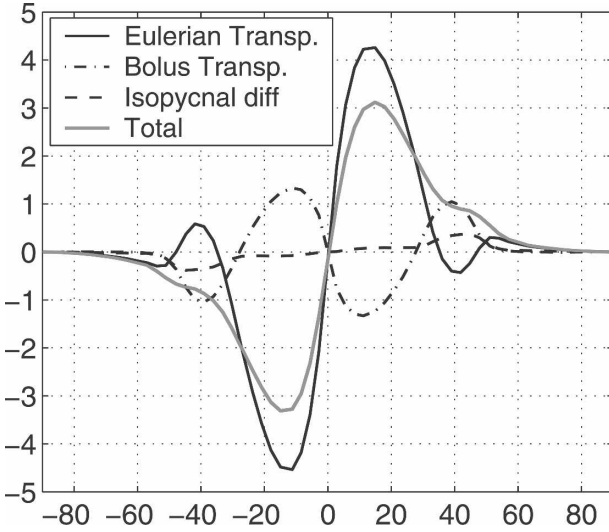
FIG. 7. Terms contributing to the total ocean heat transport (PW): Eulerian, bolus, and diffusive contributions.
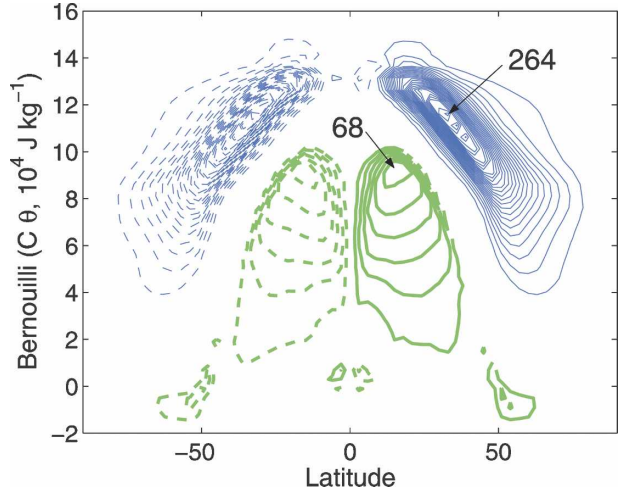

FIG. 8. Mass transport in energy coordinates derived on the aquaplanet. The contour interval is 10 Sv. Positive contours indicate a clockwise sense of overturning circulation. This should be compared to Fig. 9 of Czaja and Marshall (2006), which shows the same fields computed from analyzed fields of the current climate. Note that ΔB has the same scale in both fluids, but the absolute value is arbitrary: it has been chosen so that the overturning cells in the respective fluids conveniently lie over one another.

port is to understand the distribution of mass transport in energy coordinates. In particular the ratio of heat transports in the respective fields can be written heuristically as

$$\frac{H_A}{H_O} = \frac{\Psi_{A_{\text{res}}}}{\Psi_{O_{\text{res}}}} \times \frac{\Delta B_A}{\Delta B_O}, \qquad (9)$$

where $\Psi_{A,O_{\text{res}}}$ is the meridional mass transport in the two fluids and ΔB is the vertical change in energy (moist static energy in the atmosphere and internal energy in the ocean) across the respective meridional overturning circulations.

Figure 8 plots $\Psi_{A_{\text{res}}}$ and $\Psi_{O_{\text{res}}}$ in energy coordinates from the aquaplanet coupled model—the method of calculation is described in Czaja and Marshall (2006), where it is applied to analyzed fields. Here model output rather than analyzed fields are used. First, note that the residual meridional cell in the atmosphere extends from the equator to the pole and is dominated by eddy driven transport in mid–high latitudes (cf. Fig. 2a,b, right). Second, we see that although the energy contrast across the meridional cells in the atmosphere and ocean is rather similar in the midlatitudes, the atmospheric mass transport dominates (by a factor of 4) over the ocean mass transport. This is the key to understanding why the atmosphere plays such a dominant role in heat transport in the extratropics.

To arrive at a more quantitative understanding, let us return to the zonal-average residual momentum balance in the two fluids that can be written as

$$-f v_{\text{res}} = f \frac{\partial \psi_{\text{res}}}{\partial z} = \frac{1}{\rho}\left(\frac{\partial \tau}{\partial z} + \frac{\partial \tau_e}{\partial z}\right) + \text{Reynold Stress}.$$

Integrate from the surface, where $\tau = \tau_s$ and $\tau_e = 0$, across the planetary boundary layers of the two fluids to where $\tau = 0$, neglecting Reynolds stress processes in both fluids, we obtain the following:

$$f\psi_{A_{\text{res}}} = \frac{1}{\rho_A}(-\tau_s + \tau_{A_e}) \text{ Atmosphere}$$

$$-f\psi_{O_{\text{res}}} = \frac{1}{\rho_O}(\tau_s - \tau_{O_e}) \text{ Ocean}.$$

Adding the two together we find

$$f(\Psi_{A_{\text{res}}} - \Psi_{O_{\text{res}}}) = \tau_{A_e} - \tau_{O_e}, \qquad (10)$$

where $\Psi_{A_{\text{res}}} = \rho_A \psi_{A_{\text{res}}}$ and $\Psi_{O_{\text{res}}} = \rho_O \psi_{O_{\text{res}}}$ are the mass transports in the two fluids. We now consider two limit cases.

1) In the mid–high-latitude atmosphere, the residual flow is dominated by eddy processes, so that $\tau_{A_{\text{eddy}}}/f\Psi_{A_{\text{res}}} \to 1$ and Eq. (10) reduces to

$$\frac{\Psi_{A_{\text{res}}}}{\Psi_{O_{\text{res}}}} \to \frac{\tau_{A_{\text{eddy}}}}{\tau_{O_{\text{eddy}}}}. \qquad (11)$$

Residual-mean theory tells us that the eddy stresses are related to eddy fluxes as in Eq. (3). Moreover, relating the eddy fluxes to large-scale gradients us-

ing eddy diffusivities for the respective fluids, Eq. (11) becomes[4]

$$\frac{\Psi_{A_{\text{res}}}}{\Psi_{O_{\text{res}}}} \to \frac{\rho_A K_A |s_{\theta_A}|}{\rho_O K_O |s_{\rho_O}|}, \tag{12}$$

where s_{ρ_O} and s_{θ_A} are, respectively, the slopes of the buoyancy surfaces in the ocean and the slope of isentropic surface in the atmosphere. Inspection of the mean $\overline{\theta}$ and $\overline{b}$ fields in the subtropical regions of the atmosphere and ocean (between latitudes of $30° \to 60°$), yields isentropic slopes of $|s_{\theta_A}| \sim |s_{\rho_O}| \sim 10^{-3}$. The eddy diffusivities if the respective fluids are (diagnosed) $K_A = 4 \times 10^6$ m^2 s^{-1} in the atmosphere and (prescribed) 800 m^2 s^{-1} in the ocean. Thus Eq. (12) yields $\Psi_{A_{\text{res}}}/\Psi_{O_{\text{res}}} \sim 5$: an atmospheric mass transport that is 5 times greater than that in the ocean. We have already noted that in the midlatitudes the energy contrast across the atmospheric and oceanic cells are similar to one another ($\Delta B_A/\Delta B_O \to 1$) and so Eq. (9) tells us that $H_A/H_O \to \Psi_{A_{\text{res}}}/\Psi_{O_{\text{res}}} \sim 5$, thus, a large factor.

2) As the equator is approached, eddy processes become increasingly small in both fluids and so, setting $\tau_{A_{\text{eddy}}}, \tau_{O_{\text{eddy}}} \to 0$, Eq. (10) yields $\Psi_{O_{\text{res}}}/\Psi_{A_{\text{res}}} \to 1$, the result employed by Held (2001). Thus, Eq. (9) tells us that $H_A/H_O \to \Delta B_A/\Delta B_O$. In the Tropics the vertical gradient of moist static energy in the atmosphere is eroded by moist convection [see the moist potential temperature plotted in Fig. 2a (top left)], whereas the tropical ocean thermocline is maintained strong by upwelling of deep water toward the surface. Thus, $H_A/H_O \sim \Delta B_A/\Delta B_O \to 0$, a rationalization of why the tropical ocean carries more heat poleward than the tropical atmosphere.

Before going on to a discussion of the variability of the coupled system, it is important to note that the mean climate of the aquaplanet solution reported here is rather different from that of Smith et al. (2006). Smith et al. report a very warm climate without ice caps and a diffuse thermocline reaching down to 3 km or so and abyssal temperatures of some 18°C. Although a much more sophisticated atmospheric model is employed by Smith et al. (2006), we speculate that ocean model formulation is the major cause of these differences. They employ strong horizontal (and hence necessarily) diapycnal mixing of T and S and find that diffusive processes dominate ocean heat transport in the mid–high latitudes. A full 1 PW of heat is diffused poleward in the ocean at $\pm 60°$, evidently melting the ice. Once the ice has melted, the ice-albedo feedback disappears and, in its absence, the coupled system moves in to a much warmer climate. In contrast, in the present simulation with a more physically based representation of eddy processes (Gent and McWilliams 1990), which likens eddy transfer to an advective, rather than a diffusive process, diffusion plays a negligible role in the meridional heat transport (see Fig. 7). At $\pm 60°$ the meridional ocean heat flux is only 0.1 PW and is entirely advective. Ice remains at the Pole during the whole period of the 4000-yr integration.

3. Variability of the coupled climate

a. Coupled aquaplanet climate variability

The climate of the aquaplanet shows considerable variability. Its primary source is stochastic forcing by midlatitude synoptic-scale systems. To study the nature of the variability, we performed an empirical orthogonal function (EOF) analysis of the zonally and yearly averaged fields of the coupled simulation. The analysis was carried out poleward of 20°S using 1000 yr of data. Figure 9 shows the first EOFs of the zonal wind/current and meridional circulation of the ocean and atmosphere. The principal components (PC) have been normalized to unit variance so that their EOFs are in physical units and correspond to one standard deviation of the PC.

In each of these fields, variability is dominated by the first EOF, which captures between 58% and 87% of the total variance (the second mode explains less than 17% of the variance). The four modes shown in Fig. 9 covary at zero lag with correlations of 0.9 or higher. The zonal wind mode, a dipole centered at about 50°S, represents a meridional displacement of the jet stream. We will call the phase shown in Fig. 9 the positive phase because it corresponds to a poleward shift of the jet. The meridional shift of the jet is associated with an anomalous meridional circulation largely driven by eddy momentum fluxes (see Robinson 1991; Hartmann and Lo 1998; Watterson 2000), which are balanced by Ekman friction at the ground. The anomalous zonal winds also drive a meridional circulation in the ocean through Ekman pumping (as seen in the third panel of Fig. 9). As expected from the continuity of the stress at the air–sea interface, the meridional circulation in the ocean and atmosphere are comparable in strength. The first zonal current mode captures the fast barotropic response of

---

[4] Note, a downgradient flux relationship is employed in our ocean model to parameterize eddy fluxes that make up the bolus transport ψ^* [see Eq. (3)]. Our atmospheric model resolves fluxes due to synoptic-scale systems. Nevertheless, conceptually, it is still useful to express the transfer properties of synoptic eddies in terms of a diffusivity.
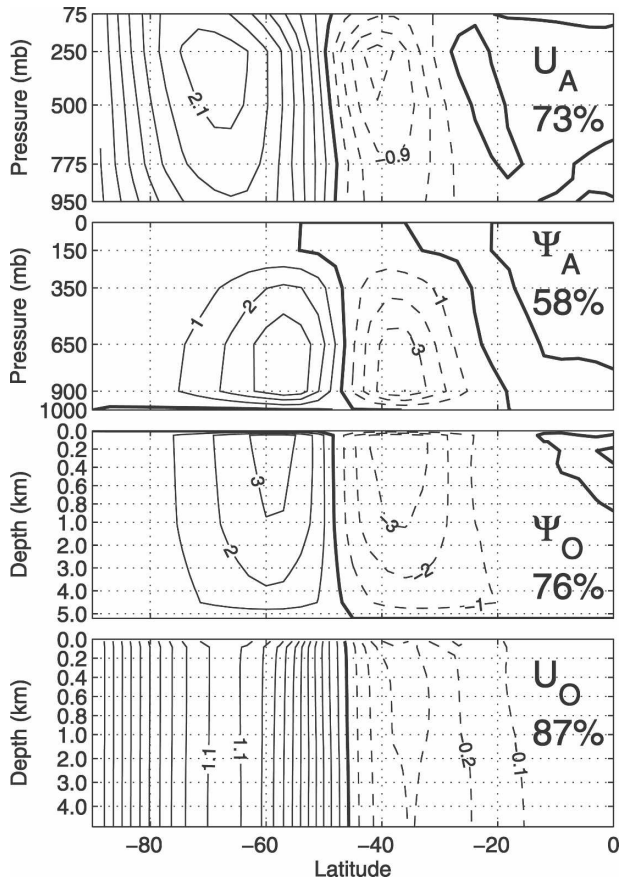
FIG. 9. (top to bottom) First EOFs of zonal wind (m s^{-1}), atmospheric meridional streamfunction (Sv), oceanic streamfunction (Sv), and zonal current (cm s^{-1}). Annually averaged data from 1000 yr of the coupled run were used, detrended before analysis. A positive overturning streamfunction denotes a clockwise circulation.

the ocean to surface wind fluctuations: variability in the ocean simply mirrors atmospheric jet fluctuations moving meridionally in phase with the forcing.

Figure 10 shows the spectrum and autocorrelation of the PC associated with the first zonal wind EOF (top panel of Fig. 9). The spectrum is almost white with a slight peak at a period of around 10 yr. Consistently, the autocorrelation decreases sharply with lag with a (small) negative lobe at a lag of 4 yr. Also shown in Fig. 10 is the autocorrelation of surface air temperature. The spectra and autocorrelation of the PCs associated with the other modes shown Fig. 9 are very similar to those shown in Fig. 10.

In Fig. 11 we regress the ocean temperature on to the PC of the first atmospheric mode at various lags. At lag 0, the temperature anomaly associated with the atmospheric mode is a dipole. The equatorward propagation of the positive pole is particularly striking while the

negative pole at about 35°S appears to be subducted and advected poleward below the surface. Although this negative anomaly is strongly damped, there is an indication it upwells near 50°S at lag 3. This pathway is consistent with the time-averaged residual-mean circulation (plotted in blue in the lag 3 panel).

The positive pole is advected at about 1.1 cm s^{-1} (15° latitude in 5 yr). However, the straight line superimposed on Fig. 11, shows that this velocity is not uniform: the anomaly seems to move faster between lags 1 and 3, and slower between lags 0 and 1 and lags 4 and 5.

To identify the processes that force SST anomalies, in Fig. 12 the surface heat flux anomalies and anomalous Ekman advection are regressed on to the PC of the first zonal wind EOF at lag −1, 0, and 1. The Ekman contribution ($V'_{ek}\partial_y \overline{T}$) has been converted to a surface heat flux (in W m^{-2}). By convention, a positive heat flux is downward (warming the SST). Clearly, annual averages are not ideal for such an analysis since the time scales associated with these forcings are typically a month. Nevertheless, at lag 0 we observe that Ekman advection forces the SST anomaly. Poleward of 50°S, the anomalous easterlies generate Ekman currents directed poleward (see Fig. 9), which advects cold waters and cools the SST while the opposite holds equatorward of 50°S. The surface heat flux is observed to damp the SST anomalies at lag −1. Thus, in the aquaplanet, the surface heat flux does not participate in the creation of midlatitude SST anomalies. Instead they are induced by Ekman advection. Note that south of 60°S we do not observe strong SST anomalies because of the presence of sea ice that shields the ocean from surface heat fluxes. Moreover, the mean SST has no gradients (uniform temperature at the freezing point of −1.8°C), thus inhibiting Ekman advection.

Returning to Fig. 11, we conclude that SST anomalies are forced by the anomalous wind fields through Ekman advection, damped by surface heat flux, and advected equatorward by the mean surface flow. After a time $L/(2V)$ (L is the wavelength of the SST anomaly, $L/2$ is the distance between the anomaly centers, and V is the surface velocity), the SST anomaly is similar to that seen at lag 0, but with a reversed sign. If the atmospheric forcing had not changed phase, the Ekman advection would then damp the SST anomaly. However, the atmospheric standing mode, having a nearly white spectrum, contains energy at the period L/V and changes sign every $L/(2V)$, thus leading to a positive feedback on the SST anomaly, the spatial resonance mechanism of Saravanan and McWilliams (1998). We thus observe a spectral peak at period near $L/V \sim 10$ yr (if $L = 30°$ of latitude and $V = 1$ cm s^{-1}). This can
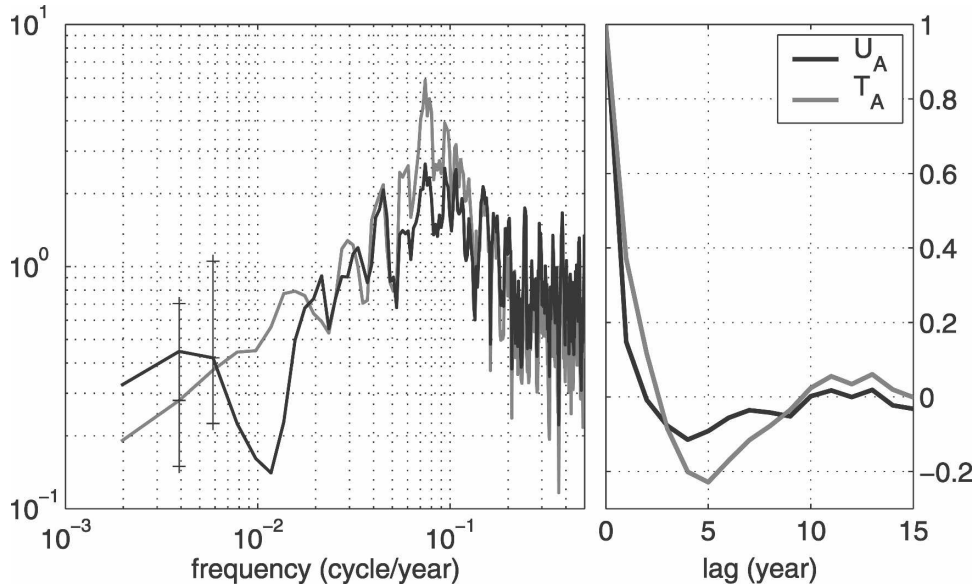
FIG. 10. Spectra and autocorrelations of the PCs associated with the first EOFs of zonal wind (black lines) and air temperature (gray lines).

be clearly seen in the spectra of SST EOFs shown in Fig. 13.

As in Saravanan and McWilliams (1998), this mechanism does not require a feedback onto the atmosphere. However, there is a hint of a preferred time scale at decadal period even in the atmosphere (see Fig. 10). This can only occur through surface heat fluxes associated with SST anomalies. The SST anomalies are generated by Ekman advection and damped by surface heat fluxes, warming/cooling the atmosphere above them. Figure 14 shows the regression of air temperature onto the PC of the first zonal wind EOF at various lags. The air temperature anomaly associated with the atmospheric mode (lag 0) is rather complex. But, in the band of strong air–sea interaction, 60°–30°S, it comprises a large positive anomaly over the height of the troposphere and a negative anomaly in the stratosphere at about 50°S. In comparison with Fig. 11, we observe that as the positive SST anomaly moves equatorward it is damped, drawing heat from the atmosphere. At lag 0, there is a small positive air temperature anomaly near the surface at 50°S. By lag 2, this anomaly has expanded upward over the entire air column. At lag 3, there is a hint of the air temperature pattern associated with a negative phase of the annular mode (i.e., opposite to lag 0). This pattern has a negative air temperature anomaly over the troposphere in the 60°–30°S band. It seems that the small positive air temperature generated by the decay of the SST negative pole favors the estab-
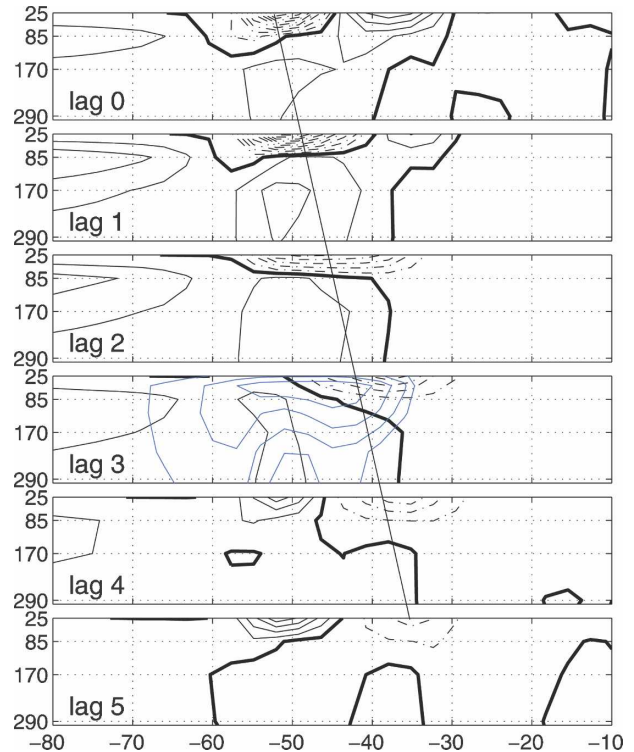

FIG. 11. Regression of the ocean temperature on to the PC of the first zonal wind EOF at different lags (in years) over the top 300 m or so of the ocean. A positive lag indicates the atmosphere leads the ocean. The blue contours indicate the averaged residual streamfunction in Sv. The slanting line striking through the panels joins the center of the SST anomalies and implies a speed of 1 cm s^{-1}.
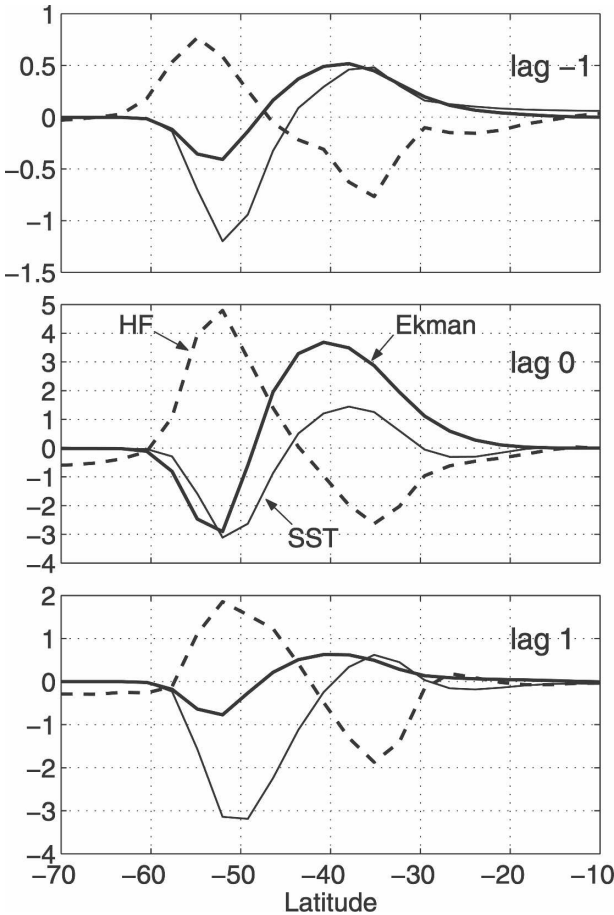
FIG. 12. Regression of the surface heat flux anomaly (W m^{-2}, dotted), and the anomalous Ekman advection ($V'_{ek}\partial_y\overline{T}$, solid black, converted to a surface heat flux), and SST anomaly (solid gray, in K multiplied by 10) onto the PC of the first zonal wind EOF at different lags in years. A positive lag indicates the atmosphere leads the ocean.

lishment of a positive phase of the annular mode. We see, then, that the emerging negative phase of the SST dipole (lag 3 or 4) is associated with a small positive feedback on to the atmosphere. The following is a summary of this process:

1) Atmospheric variability on the aquaplanet is dominated by a stochastic-in-time, fixed-in-space atmospheric mode that describes the meridional displacement of the jet. This mode drives fluctuations of the meridional overturning cells in the atmosphere and ocean and generates SST and thermal anomalies through Ekman advection on a scale L set by the wind stress anomaly.

2) The SST and associated thermal anomalies are damped by surface heat fluxes and advected by the mean residual flow in the ocean. A preferred time scale on the order of L/V arises through the spatial

resonance mechanism identified by Saravanan and McWilliams (1998). This time scale can readily be seen in the SST spectra and autocorrelations shown in Fig. 13.

3) The time scale L/V then imprints itself on atmospheric and oceanic fields. Decadal variability observed in the atmosphere is indicative of a slight feedback between the atmosphere and ocean (see Fig. 10). This occurs via surface heat flux through the damping of SST and near-surface thermal anomalies as they are advected meridionally by the residual-mean meridional circulation. Decadal variability of the interior ocean is a consequence of subduction of thermal anomalies created at the surface as described in the previous point.

b. Simple model

We consider a highly idealized model: a zonal-mean atmosphere–ocean extending between $y = 0$ and $y = L$ (corresponding to the 60°–30°S band of latitude, i.e., $L = 3300$ km). A simple equation for the time evolution of the SST anomaly [$T'(y, t)$] represents advection by the mean residual surface current ($\overline{V}_{res}$), advection of the mean temperature ($\overline{T}$) by the anomalous Ekman current (V'_{ek}), and a linear damping (λ) associated with air–sea heat fluxes and other processes:

$$\partial_t T' + \overline{V}_{res}\partial_y T' = -V'_{ek}\partial_y\overline{T} - \lambda T'. \quad (13)$$

The Ekman current is expressed in terms of the surface wind stress τ'_x:

$$V'_{ek} = -\frac{\tau'_x}{\rho_o fH}, \quad (14)$$

where H is the thickness of the surface oceanic layer.

We suppose that the wind stress has two components:

1) one due to internal atmospheric dynamics independent of the ocean state, modeled as a white noise process in time but with a large-scale standing pattern in space: $N(t)\sin(2\pi y/L)$; and

2) a second (smaller) contribution induced by SST anomalies: $-\alpha T'$. The SST feedback on to the atmosphere is represented by a linear coefficient α, as in Marshall et al. (2001).

Hence we write

$$\tau'_x = N - \alpha T'. \quad (15)$$

The model set out in Eqs. (13), (14), and (15) yields an SST spectrum given by (see appendix B for details of the calculation):
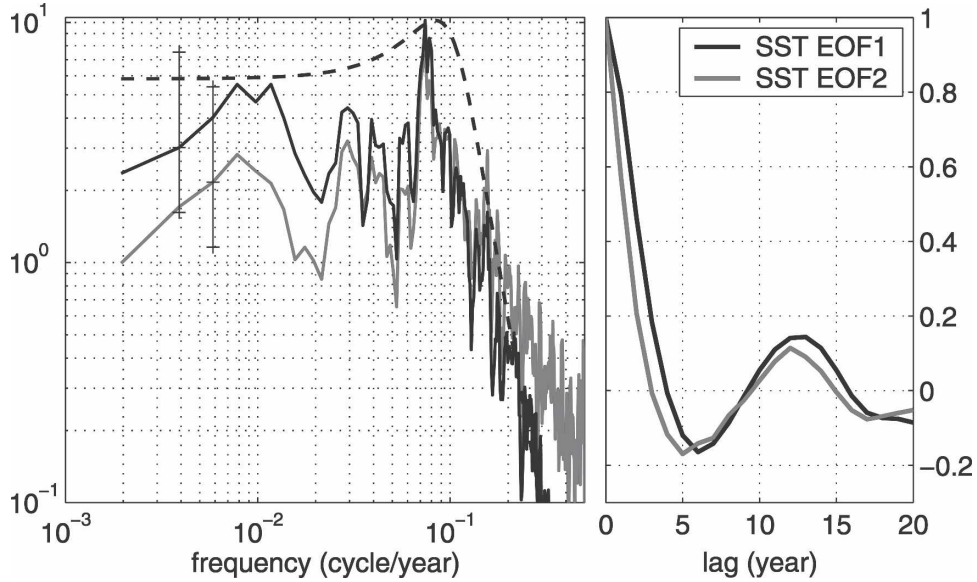
FIG. 13. Spectra and autocorrelation of the first two EOFs of SST. The dotted line plots the theoretical spectrum, Eq. (16), for $\Gamma = 0.5$ and $V_{\text{res}}k = 1.9 \times 10^{-8}$ s^{-1}.

$$|\tilde{T}|^2 = \frac{\delta^2|\tilde{N}|^2}{k^2\overline{V}_{\text{res}}^2} \frac{1}{\left[1 - \left(\dfrac{\omega}{k\overline{V}_{\text{res}}}\right)^2 + \Gamma^2\right]^2 + 4\left(\dfrac{\omega}{k\overline{V}_{\text{res}}}\right)^2\Gamma^2},$$

(16)

where $\tilde{T}$, $\tilde{N}$ are the amplitudes of the Fourier components of the temperature and forcing [see Eq. (A1)] at frequency ω, δ is a (negative) coefficient scaling the wind stress into an SST forcing and

$$\Gamma = \frac{\lambda_{\text{eff}}}{k\overline{V}_{\text{res}}}$$

(17)

is a ratio of advective and damping time scales. Here k is the meridional wavenumber of the forcing, λ_{eff} is the effective damping rate, which combines the heat flux feedback, λ, and the atmospheric feedback, α [see Eqs. (A3)].

If N has a white spectrum, $|\tilde{N}|^2$ is then independent of the frequency, and the spectrum has a maximum when the denominator is minimum, which occurs for

$$\left(\frac{\omega_m}{k\overline{V}_{\text{res}}}\right)^2 = 1 - \Gamma^2.$$

(18)

Therefore, a spectral peak only exists if $\Gamma < 1$: that is, if the damping time scale is longer than the advective time scale. If such conditions pertain, the spectral peak is obtained at periods somewhat longer than the advective time scale to a degree that depends on the damping time. For $\lambda_{\text{eff}} \to 0$, we find the intuitive results that the peak occurs at the period $T = 2\pi/\omega = L/\overline{V}_{\text{res}}$.

To proceed further we must compare $k\overline{V}_{\text{res}}$ to the damping time scale $(\lambda_{\text{eff}})^{-1}$, Eq. (A3), which depends on both λ and δ. Let us first determine the contribution to λ from air–sea heat fluxes. Following Frankignoul et al. (1998), we assume that the air–sea heat flux anomaly Q' can be decomposed, thus,

$$Q' = N - aT',$$

(19)

where N is independent of the SST anomaly and a is the heat flux feedback in W m^{-2} K^{-1}. Multiplying through by T', the covariance R_{TQ} at lag τ between Q' and T' is given by

$$R_{TQ}(\tau) = R_{TN}(\tau) - aR_{TT}(\tau),$$

(20)

where T leads Q if $\tau > 0$.

In extratropical latitudes, N, which is solely controlled by intrinsic atmospheric dynamics, can be modeled by a short time-scale random process. We can then assume that R_{TN} vanishes for lags longer than the atmospheric persistence yielding

$$a \simeq -\frac{R_{TQ}}{R_{TT}}.$$

(21)

From 50 yr of monthly and zonally averaged SST and air sea heat flux anomalies, a has been estimated at lags of -3 and -2 months as a function of latitude (not shown). It varies between 5 and 15 W m^{-2} K^{-1}. We choose 10 W m^{-2} K^{-1} as a typical value, giving $\lambda = a/(\rho_o c_o H) = 2.4 \times 10^{-8}$ s^{-1} $\simeq (1.2$ yr$)^{-1}$ if H is 100 m.
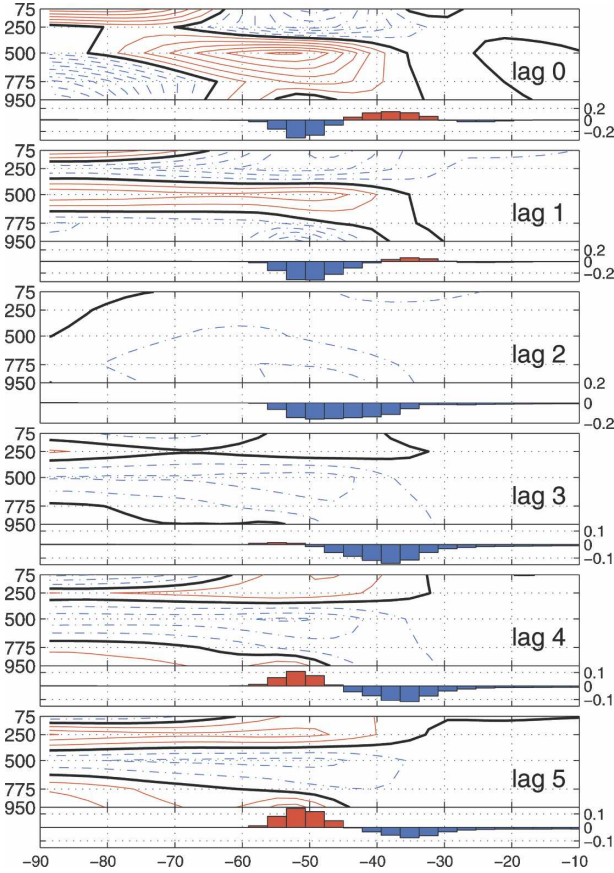
FIG. 14. Regression of the air temperature (contours) and SST (bars) anomalies onto the PC of the first zonal wind EOF at different lags (in years). The zonal wind leads air temperature and SST for positive lags. For air temperature, the negative and positive contours are blue dashed and red solid, respectively. The zero contour is highlighted; the contour interval is 0.1 K at lag 0 and 0.05 K otherwise. Note the changing range of the SST scale.

If we assume $\alpha = 0$ in Eq. (A3), then if $V_{res}k = 1.9 \times 10^{-8}$ s^{-1} we find that $\Gamma \sim 1.4$ and there is no peak in the spectrum given by Eq. (16).[5] We therefore consider the effect of the atmospheric feedback term, α in Eq. (19).

The magnitude of α can be estimated in a similar manner by multiplying Eq. (15) through by T:

$$\alpha \simeq -\frac{R_{T\tau_x}}{R_{TT}}. \qquad (22)$$

---

[5] Note that although the heat flux feedback is probably the main contribution to λ, other contributions have been neglected here: diffusion (a damping), reemergence of the temperature anomalies around 60°S (a positive feedback), and anomalous advection by the bolus velocity which sustains SST anomalies (also a positive feedback). Thus, our λ may be slightly overestimated here.

Since τ'_x represents the atmospheric annular mode, we first compute the EOFs of the monthly and zonally averaged zonal wind stress. Once again the annular mode is the leading mode of variability (explaining 65% of the variance). The feedback onto the atmospheric circulation is due to large-scale rather than local SST anomalies, and so we also compute the monthly and zonally averaged EOFs of SST. The second mode is a dipole forced by the annular variability, just as obtained using yearly data. We estimate the feedback of this mode onto the atmosphere using the above equation and obtain $\alpha = 0.2$. This corresponds to a 0.2 deviation of the annular mode PC for a unit deviation of the SST PC. The amplitude of the annular mode is typically 0.02 N m^{-2} while that of the SST dipole is 0.2 K, giving $\alpha = 0.02$ N m^{-2} K^{-1}. Thus, if $\delta = 7.7 \times 10^{-7}$ [assuming $f = 10^{-4}$ s^{-1}, $H = 100$ m, $\partial_y \overline{T} = 7 \times 10^{-6}$ K m^{-1} and using Eq. (A2)] we find that $\lambda_{eff} = \lambda + \delta\alpha = 0.87 \times 10^{-8}$. This implies a $\Gamma = 0.5$ and so we ought to observe a peak in the SST spectrum. Indeed we do. The dotted line in Fig. 13 plots the theoretical spectrum, Eq. (16), for $\Gamma = 0.5$ and $Vk = 1.9 \times 10^{-8}$ s^{-1}, against the observed spectrum of the leading two EOFs of SST.

We conclude that the slight feedback of SST anomalies on the overlying atmospheric wind stress, Eq. (15), is essential in acting to reduce (by a factor of 2) the damping rate of SST anomalies in Eq. (A3) due to air–sea heat fluxes.

4. Conclusions

We have described the climate and variability found in a numerical simulation of an aquaplanet. The atmospheric state is reminiscent of that of the present climate. It comprises baroclinically unstable subtropical jets, a Hadley circulation, midlatitude surface westerlies, and trade winds in the Tropics. The ocean circulation, however, is very different from our own. In the absence of meridional barriers, it comprises zonal jets that follow the direction of the prevailing surface stress. The dynamics is captured by the residual-mean theory of Marshall and Radko (2003) in which the depth of the thermocline is controlled by eddy dynamics. The extratropical ocean circulation has a dynamics that is somewhat analogous to that of the present-day Antarctic Circumpolar Current. The Eulerian-mean flow is almost completely cancelled by the eddy bolus transport. Outcropping isopycnals at these high latitudes dive down deep into the interior ocean only to outcrop in the other hemisphere. Ocean mixing processes thus act on rather weak interior stratification and so cannot support a significant residual circulation on isopycnals that

only outcrop at high latitudes. At lower latitudes, however, subducted isopycnal surface are drawn right up toward the surface in the same hemisphere to form the tropical thermocline. Mixing processes acting on the strong tropical stratification can now support a significant residual circulation. These are the aquaplanet's analogy of subtropical cells, driven by the trade winds with eddy processes playing a secondary role.

Study of the meridional heat transport on the aquaplanet reveals that the above properties of the meridional overturning circulation of the ocean are key to its ability to transport heat meridionally. The vigorous subtropical cells are very active transporters of heat, the weak (residual) overturning cells of mid–high latitudes very inefficient in transporting heat. This inability of the ocean to transport heat to polar latitudes leads to the formation of polar ice caps, which is a primary feature of the aquaplanet climate. The polar ice has a major impact on the planetary albedo and demands that the coupled system transport a very significant amount of heat poleward (~8 PW) to maintain equilibrium.

The simulated partition of heat transport between the atmosphere and ocean on the aquaplanet is remarkably similar to the present climate. We have argued here (and elsewhere—Czaja and Marshall 2006) that this is a consequence [see Eq. (9)] of very robust properties of the coupled system: in tropical latitudes, the parity of meridional mass transports in the two fluids in tropical latitudes but dominance of oceanic stratification over that of the atmosphere; in mid–high latitudes, the dominance of atmospheric meridional mass transport over that of the ocean, with roughly equal energy differences across these circulations. It is hard to conceive of a climate in which these properties of the respective stratifications and mass transports could be very different. Hence we conclude that gross features of the partition of heat transport between the atmosphere and ocean are very robust.

A focus of our study has been the variability of the aquaplanet climate and the extent to which that variability is coupled. In the absence of a meridional boundary, there can be no tropical warm pool or cold pool and so the ENSO phenomenon is absent. Variability is driven from the midlatitudes via atmospheric annular modes that are internally generated through the interaction of the atmospheric storm track with the zonal flow. This manifests itself as a "wobbling" of the midlatitude jet stream and its associated surface wind stress. Variability in the zonal stress acting on the ocean drives variability in the strength of the oceanic zonal jets creating annular modes in the ocean. We observe strong coherence between the zonal jets in the atmosphere and ocean at all time scales.

The stochastic-in-time, fixed-in-space variability is imposed on the underlying ocean driving the SST variability. Through the mechanism described in Saravanan and McWilliams (1998), coupled variability becomes enhanced in power at decadal time scales given by L/V, where V is the strength of the mean meridional ocean current advecting anomalies and L is the lateral scale of the Ekman forcing generating those SST anomalies. Remarkably this decadal time scale feeds back on the atmosphere above, coloring the spectrum of atmospheric variability giving it a slight, but not insignificant, enhancement of power at decadal time scales. It is not clear whether the coupled mechanism explored here is at work in the present climate, although if it were, the Southern Ocean would be a likely place to study.

Finally one might hope that the key features of the aquaplanet climate described here might be somewhat insensitive to model formulation and implementation details. Unfortunately, the only other published result—that of Smith et al. (2006)—finds a very different climate state. As discussed in section 2c, we believe differences in ocean model formulation are the primary reason for these discrepancies. Further study with different models will be required to determine whether this is indeed the case. Perhaps a coupled aquaplanet model intercomparison project is called for, in the spirit of Neale and Hoskins (2000), but in which the ocean beneath is allowed to move.

We are currently using the aquaplanet climate as a reference solution for coupled calculations of the kind described in Smith et al. (2006), in which the ability of the ocean to transport heat around the globe is placed under geometrical constraints by the introduction of, for example, meridional boundaries with and without gaps.

APPENDIX A

Details of the Coupled Atmosphere–Ocean General Circulation Model

a. Details of the coupled atmosphere–ocean general circulation model

The coupled model is constructed using a single dynamical core—that of the MITgcm (Marshall et al. 1997a,b)—in which isomorphisms are used to render

atmospheric and oceanic counterparts, as described in Marshall et al. (2004). The coupled model is run forward on the cubed sphere described in Adcroft et al. (2004).

b. Atmospheric physics

The physics package developed by Molteni (2003) is well suited to exploratory climate simulation and based on the same physical principles as "state of the art" models. It is sufficiently concise that a single person can grasp it in its entirety but, as illustrated in section 4, exhibits considerable realism. Briefly, it utilizes the following limited set of modules parameterizing key processes.

1) SURFACE FLUXES OF MOMENTUM AND ENERGY

Fluxes are defined by bulk aerodynamic formulas with different exchange coefficients between the land and sea. Coefficients for (sensible and latent) heat fluxes also depend on the vertical gradient of potential temperature between the surface and the lowest model level.

2) CONVECTION

A simplified mass flux scheme is activated when conditional instability is present [namely, where saturation moist static energy decreases with height between the planetary boundary layer (PBL) and the two upper-tropospheric layers], and where relative humidity in the PBL exceeds a fixed threshold. The cloud-base mass flux (at the top of the PBL) is such that the PBL relative humidity is relaxed toward the threshold value. Detrainment occurs only at the cloud-top level (determined by the conditional instability criterion), while entrainment occurs in the lower troposphere if the cloud top is at the highest tropospheric level. The air in the updrafts is assumed to be saturated.

3) LARGE-SCALE CONDENSATION

When relative humidity exceeds a fixed threshold, specific humidity is relaxed toward the corresponding threshold value, and the latent heat content removed from the atmosphere is converted into dry static energy.

4) CLOUD COVER

Cloud cover is determined diagnostically from the maximum relative humidity in an air column including all tropospheric layers except the PBL.

5) SHORTWAVE RADIATION

Shortwave (SW) radiation is reflected by clouds at the top of the troposphere and at the surface; the cloud albedo is proportional to the total cloud cover. The SW transmissivity is a function of layer mass, specific humidity, and cloud cover.

6) LONGWAVE RADIATION

A four-band longwave (LW) scheme is used, one for the atmospheric "window" and the remaining four for the absorption by water vapor and carbon dioxide, dependent on the mass and humidity of the layers.

7) VERTICAL DIFFUSION (SHALLOW CONVECTION)

Vertical diffusion only acts between the two lowest model layers. Dry static energy and specific humidity are diffused when a conditional instability criterion is satisfied. Otherwise, only humidity is diffused, at a slower rate.

APPENDIX B

Solution of the Idealized Coupled Model

In the spirit of Saravanan and McWilliams (1998), combining Eqs. (13), (14), and (15), and taking the Fourier transform, leads to

$$(-i\omega + \lambda_{\mathrm{eff}} + \overline{V}_{\mathrm{res}}\partial_y)\tilde{T} = \delta\tilde{N}\sin(ky), \qquad \text{(B1)}$$

where $\tilde{T} = \tilde{T}(\omega, y)$ and $\tilde{N} = \tilde{N}(\omega)$, and

$$\delta = \frac{\partial_y\overline{T}}{\rho_o f H} \qquad \text{(B2)}$$

is a (negative) coefficient scaling the wind stress into an SST forcing, and

$$\lambda_{\mathrm{eff}} = \lambda + \delta\alpha \qquad \text{(B3)}$$

is the effective damping combining the heat flux feedback λ and the (scaled) atmospheric feedback α. Since δ is negative, the effective damping is smaller than λ if $\alpha > 0$.

Equation (B1) can further be simplified to

$$\left(\frac{1}{k}\partial_y + A\right)\tilde{T} = B\sin(ky), \qquad \text{(B4)}$$

where $A = (\lambda_{\mathrm{eff}} - i\omega)/k\overline{V}_{\mathrm{res}}$ and $B = \delta\tilde{N}/k\overline{V}_{\mathrm{res}}$.

We know the solution is of the following form:

$$\tilde{T} = a_1 e^{-Ay} + a_2 \cos(ky) + a_3 \sin(ky). \qquad \text{(B5)}$$

The coefficients a_2 and a_3 are determined by substituting the form (B5) into Eq. (B4), while a_1 is obtained from the boundary condition $T'(0, t) = 0$ (since at the sea ice edge SST variability is close to zero). The solution is then

$$\tilde{T} = \frac{B}{1 + A^2} [e^{-Aky} - \cos(ky) + A \sin(ky)],$$

(B6)

and is made up of two parts: the first $B/(1 + A^2)$ factor only depends on frequency, the second term in square brackets includes a spatial modulation. Equation (16) is the spectrum of the frequency-dependent first term.

REFERENCES

Adcroft, A., J.-M. Campin, C. Hill, and J. Marshall, 2004: Implementation of an atmosphere–ocean general circulation model on the expanded spherical cube. *Mon. Wea. Rev.,* **132,** 2845–2863.

Barsugli, J. J., S. Shin, and P. D. Sardeshmukh, 2005: Tropical climate regimes and global climate sensitivity in a simple setting. *J. Atmos. Sci.,* **62,** 1226–1240.

Charney, J. G., E. Kalney, E. Schneider, and J. Shukla, 1988: A study of the dynamics of the ITCZ in a symmetric atmosphere-ocean model. NASA Tech. Memo. 86220, 15 pp.

Czaja, A., and J. Marshall, 2006: The partitioning of poleward heat transport between the atmosphere and ocean. *J. Atmos. Sci.,* **63,** 1498–1511.

Ferreira, D., J. Marshall, and P. Heimbach, 2005: Estimating eddy stresses by fitting dynamics to observations using a residual-mean ocean circulation model. *J. Phys. Oceanogr.,* **35,** 1891–1910.

Frankignoul, C., A. Czaja, and B. L'Heveder, 1998: Air–sea feedback in the North Atlantic and surface boundary conditions for ocean models. *J. Climate,* **11,** 2310–2324.

Gent, P. R., and J. C. McWilliams, 1990: Isopycnal mixing in ocean circulation models. *J. Phys. Oceanogr.,* **20,** 150–155.

Gill, A. E., J. S. A. Green, and A. J. Simmons, 1974: Energy partition in the large-scale ocean circulation and the production of midocean eddies. *Deep-Sea Res.,* **21,** 499–528.

Hartmann, D. L., and F. Lo, 1998: Wave-driven zonal flow vacillation in the Southern Hemisphere. *J. Atmos. Sci.,* **55,** 1303–1315.

Held, I. M., 2001: The partitioning of the poleward energy transport between the tropical ocean and atmosphere. *J. Atmos. Sci.,* **58,** 943–948.

Hess, P. G., 1993: Maintenance of the intertropical convergence zone and the large-scale tropical circulation on a water-covered earth. *J. Atmos. Sci.,* **50,** 691–713.

Kirtman, B. P., and E. K. Schneider, 2000: A spontaneously generated tropical atmospheric general circulation. *J. Atmos. Sci.,* **57,** 2080–2093.

Marshall, D., 1997: Subduction of water masses in an eddying ocean. *J. Mar. Res.,* **55,** 201–222.

Marshall, J., and T. Radko, 2003: Residual mean solutions for the Antarctic Circumpolar Current and its associated overturning circulation. *J. Phys. Oceanogr.,* **33,** 2341–2354.

——, A. Adcroft, C. Hill, L. Perelman, and C. Heisey, 1997a: A finite-volume, incompressible Navier Stokes model for studies of the ocean on parallel computers. *J. Geophys. Res.,* **102** (C3), 5753–5766.

——, C. Hill, L. Perelman, and A. Adcroft, 1997b: Hydrostatic, quasi-hydrostatic, and nonhydrostatic ocean modeling. *J. Geophys. Res.,* **102** (C3), 5733–5752.

——, H. Johnson, and J. Goodman, 2001: Interaction of the North Atlantic Oscillation with ocean circulation. *J. Climate,* **14,** 1399–1421.

——, H. Jones, R. Karsten, and R. Wardle, 2002: Can eddies set ocean stratification? *J. Phys. Oceanogr.,* **32,** 26–38.

——, A. Adcroft, J.-M. Campin, and C. Hill, 2004: Atmosphere–ocean modeling exploiting fluid isomorphisms. *Mon. Wea. Rev.,* **132,** 2882–2894.

Molteni, F., 2003: Atmospheric simulations using a GCM with simplified physical parametrizations. I: Model climatology and variability in multidecadal experiments. *Climate Dyn.,* **20,** 175–191.

Munk, W. H., 1950: On the wind-driven ocean circulation. *J. Meteor.,* **7,** 79–93.

Neale, R., and B. Hoskins, 2000: A standard test for AGCMs including their physical parametrizations. II: Results for the Met. Office model. *Atmos. Sci. Lett.,* **1,** 108–114.

Robinson, W., 1991: The dynamics of the zonal index in a simple model of the atmosphere. *Tellus,* **43A,** 295–305.

Saravanan, R., and J. C. McWilliams, 1998: Advective ocean–atmosphere interaction: An analytical stochastic model with implications for decadal variability. *J. Climate,* **11,** 165–188.

Schneider, T., K. L. Smith, P. A. O'Gorman, and C. C. Walker, 2006: A climatology of tropospheric zonal-mean water vapor fields and fluxes in isentropic coordinates. *J. Climate,* **19,** 5917–5932.

Smith, R. S., C. Dubois, and J. Marotzke, 2006: Global climate and ocean circulation on an aquaplanet ocean–atmosphere general circulation model. *J. Climate,* **19,** 4719–4737.

Thompson, D. W. J., and J. M. Wallace, 1998: The Arctic Oscillation signature in the wintertime geopotential height and temperature fields. *Geophys. Res. Lett.,* **25,** 1297–1300.

Watterson, I. G., 2000: Southern midlatitude zonal wind vacillation and its interaction with the ocean in GCM simulations. *J. Climate,* **13,** 562–578.

Winton, M., 2000: A reformulated three-layer sea ice model. *J. Atmos. Oceanic Technol.,* **17,** 525–531.